HHS Public Access

Author manuscript

*Acta Biomater*. Author manuscript; available in PMC 2016 July 15.

Published in final edited form as:

*Acta Biomater*. 2015 July 15; 21: 63–73. doi:10.1016/j.actbio.2015.04.014.

# Dendritic Nanoconjugates of Photosensitizer for Targeted Photodynamic Therapy

**Ahu Yuan**[a,b], **Bing Yang**[a], **Jinhui Wu**[b], **Yiqiao Hu**[b], and **Xin Ming**[a,*]

[a]Division of Molecular Pharmaceutics, UNC Eshelman School of Pharmacy, University of North Carolina, Chapel Hill, NC 27599, USA

[b]State Key Laboratory of Pharmaceutical Biotechnology, Nanjing University, Nanjing 210093, China

## Abstract

Application of photodynamic therapy for treating cancers has been restrained by suboptimal delivery of photosensitizers to cancer cells. Nanoparticle (NP)-based delivery has become an important strategy to improve tumor delivery of photosensitizers; however, the success is still limited. One problem for many NPs is poor penetration into tumors, and thus the photokilling is not complete. We aimed to use chemical conjugation method to engineer small NPs for superior cancer cell uptake and tumor penetration. Thus, Chlorin e6 (Ce6) was covalently conjugated to PAMAM dendrimer (generation 7.0) that was also modified by tumor-targeting RGD peptide. With multiple Ce6 molecules in a single nanoconjugate molecule, the resultant targeted nanoconjugates showed uniform and monodispersed size distribution with a diameter of 28nm. The singlet oxygen generation efficiency and fluorescence intensity of the nanoconjugates in aqueous media were significantly higher than free Ce6. Targeted nanoconjugates demonstrated approximately 16-fold enhancement in receptor-specific cellular delivery of Ce6 into integrin-expressing A375 cells compared to free Ce6 and thus were able to cause massive cell killing at low nanomolar concentrations under photo-irradiation. In contrast, they did not cause significant toxicity up to 2μM in dark. Due to their small size, the targeted nanoconjugates could penetrate deeply into tumor spheroids and produced strong photo-toxicity in this 3-D tumor model. As a result of their great cellular delivery, small size, and lack of dark cytotoxicity, the nanoconjugates may provide an effective tool for targeted photodynamic therapy of solid tumors.

## Graphical Abstract



*Corresponding author: Xin Ming, Ph.D., Division of Molecular Pharmaceutics, UNC Eshelman School of Pharmacy, 1073 Genetic Medicine Building, University of North Carolina, Chapel Hill, NC 27599, USA. Tel.: +1 919 966 4343. xming@email.unc.edu.

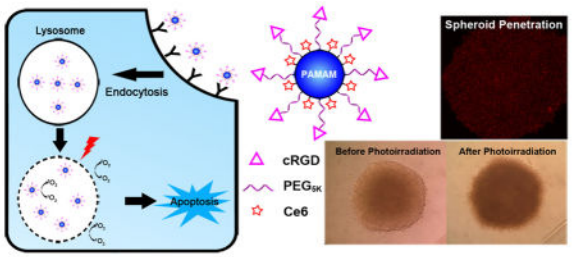


**Keywords**

Nanoconjugates; Photodynamic therapy; Targeted delivery; Tumor spheroids

## 1. Introduction

Photodynamic therapy (PDT) is a clinically approved and minimally invasive therapeutic procedure, which is based on the combined use of a photosensitizer (PS), oxygen, and light radiation. PSs are usually pharmacologically inactive in the dark and are activated by irradiation at a specific wavelength to produce reactive oxygen species (ROS), which are capable of rendering cancer cell death.[1] Clinical use of many PSs has been hampered by their intrinsic limitations including poor solubility, aggregation in aqueous solution, and poor tumor selectivity.[2] To overcome these limitations, various nanoparticles (NPs), including liposomes, inorganic NPs and polymeric NPs, have been developed to increase water solubility and enhance tumor delivery of PSs.[3–8] Among these NPs, various polymer-PS conjugates, such as Pluronic F127/Ce6 and glycol chitosan/pheophorbide A conjugates, have been reported.[9, 10] Chemical conjugation of hydrophobic photosensitizer to hydrophilic polymers allows self-assemble into NPs. Importantly, chemical conjugates demonstrate higher solubility and increased stability in vitro and in vivo than free PSs.[3–7] Further, chemical conjugation method can avoid the release of PSs from NPs before reaching to the target tissues and thus reduces side effects caused by accumulation of PSs in non-target tissues.[9, 11, 12]

Poor tumor penetration is still a limitation for NP-based delivery of PSs. For complete eradication of solid tumors, anticancer drugs including PSs should penetrate deeply in the solid tumors and reach all cancer cells in a therapeutic concentration.[13] Abraxane is a FDA-approved albumin-bound paclitaxel NP for treatment of solid tumors. Their large size (about 130 nm) allows them to preferentially accumulate in solid tumors by the Enhanced Permeability and Retention (EPR) effect.[13–15] However, although it causes lower side effects than free paclitaxel, this NP only provides modest survival benefits, likely due to poor penetration of Abraxane into deep tumor tissues.[13, 16] It has been reported that NPs smaller than 50nm may penetrate into deep tissue far from tumor vasculature.[13, 17, 18] However, most of the NPs that are used for delivery of PSs are too large for effective tumor penetration. For example, liposomes and albumin NPs that are prepared via complexation are typically larger than 100nm.[7, 19] Those prepared by chemical conjugation, though smaller than liposomes, are still larger than 50nm.[9, 10]

This study aimed to use chemical conjugation method to construct NPs that are cancer cell-selective and are smaller than 50nm. Thus, the resultant NPs can deliver PSs deeply into tumor tissues and effectively into cancer cells. For this purpose, we chose poly (amido amine) generation 7.0 (PAMAM G7) dendrimer with a diameter of 8nm as a core molecule to prepare ultra-small NPs. By modification with sufficient PEG on the surface, PAMAM dendrimers showed reduced cytotoxicity. In addition, to achieve tumor selectivity, cRGD, a ligand to integrin $\alpha_v\beta_3$ that is overexpressed in many cancer cells,[20] were functionalized to the surface of PEGylated PAMAM dendrimers. Photosensitizer Ce6 were covalently conjugated onto the RGD functionalized PAMAM and the resultant nanoconjugates (RGD-P-Ce6) were characterized in terms of size, zeta potential, fluorescence and singlet oxygen generation efficiency. We then examined cellular delivery and phototoxicity of the nanoconjugates in integrin $\alpha_v\beta_3$-expressing A375 cells, and further studied their penetration and phototoxicity in spheroids of A375 cells, a 3-D model of solid tumors.

## 2. Materials and Methods

### 2.1 Preparation of RGD-P-Ce6

PAMAM G7 (Sigma-Aldrich, St. Louis, MO) was conjugated with Mal-$PEG_{5K}$-NHS (Nanocs Inc., New York, NY) at a 1:30 molar ratio of PAMAM to PEG in PBS (pH 7.4) for 30min at room temperature, and this was followed by adding cRGDyC peptide (Peptides International, Inc., Louisville, KY) to react with the maleimide group on PEG at the ratio of RGD to PAMAM as 40:1 to obtain RGD-PAMAM (RGD-P). Ce6 (MedKoo Biosciences Inc., Chapel Hill, NC) was dissolved in DMSO, followed by the addition of 10 molar equivalents of EDC and Sulfo-NHS (Thermo Fisher, Rockford, IL). After 3 hrs, activated Ce6 (Ce6-NHS) was added into the above RGD-PAMAM solution with a 15:1 molar ratio of Ce6 to PAMAM. The reaction was gently stirred for 12 hrs in dark at room temperature. For the purification, crude nanoconjugates were chromatographed using Sephadex LH-20 (GE Healthcare, Pittsburgh, PA) to remove unreacted Ce6, and mobile phase was mixture of methanol and distilled water (v/v=1:2). After that, the resulting product was purified by gel filtration using Sephadex G100 (GE Healthcare) and PBS was used as mobile phase. In addition, monofunctional $PEG_{5K}$-NHS (Nanocs Inc.) was used for preparation of non-targeting nanoconjugates PEG-P-Ce6 with similar method (Sfig. 1).

### 2.2 Characterization of RGD-P-Ce6

The Ce6 content in the RGD-P-Ce6 nanoconjugates was measured by NanoDrop 1000 Spectrophotometer (Thermo Scientific). Free Ce6 dissolved in DMSO was used as standard solution and the amount of Ce6 of RGD-P-Ce6 (diluted with methanol) was measured as the absorption at the 405nm peak. The fluorescence of Ce6 and RGD-P-Ce6 were detected by NanoDrop 3300 (Thermo Scientific).

To evaluate the singlet oxygen generation (SOG) by light irradiation of the nanoconjugates, the singlet oxygen sensor green (SOSG, Life Technologies, Carlsbad, CA) was mixed with RGD-P-Ce6 or free Ce6 in PBS with all concentrations at 1μM. SOG was induced by irradiation at a light intensity of 3.5 $mW/cm^2$ using a 660 nm laser module diode (LaserLands, Wuhan, China) equipped with a concave lens (Edmund Optics Inc., NJ). After

irradiation, SOSG fluorescence was measured at an excitation and emission of 488nm and 525nm using FLUOstar Omega plate reader (BMG Labtech, Germany). PBS with SOSG was irradiated and served as a negative control.

The hydrodynamic sizes of the nanoconjugates were measured by dynamic light scattering using a Zetasizer Nano (Malvern Instruments, Malvern, UK). The zeta potentials were also measured using this instrument. The final Ce6 concentration of the nanoconjugates was adjusted to 20μM in DI water in these measurements. The morphology of the RGD-P-Ce6 nanoconjugates was observed using a cryo-Transmission Electron Microscope (TEM, Oberkochen, Germany). In this experiment, the nanoconjugates were diluted and dropped on 200 mesh carbon coated copper grids and were allowed to attach for 2min. Uranyl acetate aqueous solution (4%) was dropped on the grid to counterstain the nanoconjugates.

### 2.3 Cell culture and intracellular uptake

A375 cells (a non-pigmented melanoma cell line) and NIH3T3 cells (mouse fibroblasts) were cultured in DMEM medium supplemented with 10%FBS and 1% penicillin/ streptomycin at 37°C with 5% $CO_2$.

To compare the intracellular uptake, A375 cells and NIH/3T3 cells were treated with free Ce6, PEG-P-Ce6 and RGD-P-Ce6 (150nM equivalent Ce6) for 12hrs. Then the cells were trypsinized and analyzed by flow cytometry using BD LSR II, with a 405nm laser and a 670/20nm emission filter set for Ce6 fluorescence. To investigate the endocytosis pathway[21], A375 cells were pre-treated with various inhibitors (dynasore 30μM, chlorpromazine 12.5μM, filipin 5μg/ml, methyl-β-cyclodextrin 1.3mg/ml, amiloride 100μM and wortmannin 100nM) for 30 min and followed by incubation with RGD-P-Ce6 (100nM of Ce6) in the presence of the inhibitors for 4 hrs. After washing with PBS, the cells were trypsinzed and the Ce6 fluorescence intensity was measured using flow cytometry. To determine whether the cellular uptake of RGD-P-Ce6 is energy dependent, A375 cells was incubated with RGD-P-Ce6 (100nM) for 4 hrs at 4°C and the cellular uptake was compared to that at 37°C.

### 2.4 Intracellular trafficking of RGD-P-Ce6

Live cell confocal microscopy was performed to examine subcellular distribution of the targeted nanoconjugates. After cultured in glass-bottom dishes overnight, A375 cells were treated with RGD-P-Ce6 (400nM of Ce6) for 6 hrs. The cells were then treated with lysosomal marker Lysotracker Green DND-26 (75nM), ER tracker green (1μM) or transferrin-Alexa 488 (25μg/ml) for 1 hr. After washing twice with PBS, images were captured using an Olympus FV1200 confocal microscope.

### 2.5 Intracellular singlet oxygen detection after photo-irradiation

After incubated with RGD-P-Ce6 (75nM) for 12 hrs, A375 cells were further incubated with 10μM CM-$H_2$DCFDA (Life Technologies) for 60 min and were irradiated with a 660 nm laser (3.5mW/$cm^2$) for 0, 10, 20 or 30 min. After that, the cells were harvested and the fluorescence of the cells was detected by flow cytometry (FITC channel) to measure the

intracellular ROS level.[22] In addition, the intracellular ROS was also detected by observing DCF using confocal microscopy.

### 2.6 Apoptosis after photo-irradiation

After treated with RGD-P-Ce6 (50nM of Ce6) for 12 hrs, A375 cells were rinsed twice with culture medium and photo-irradiated with a 660nm laser (3.5mW/cm$^2$) for 30min. At 10min, 4hrs or 12hrs post photo-irradiation, the cells were trypsinized and then stained with Annexin V FITC/PI (Life Technologies) according to the manufacturer's instruction. The fluorescence of FITC and PI was detected with flow cytometry using a LSR II cell analyzer.

### 2.7 PDT induced lysosomal leakage

To detect the mechanism of apoptosis, lysosomal membrane permeabilization caused by photo-irradiation was visualized using confocal microscopy. After treatment of RGD-P-Ce6 (75nM) and Alexa 488-Dextran (10kD, 200μg/ml) for 4 hrs, A375 cells were rinsed with PBS and incubated for another 1 hr before photo-irradiation (660nm laser, 3.5mW/cm$^2$ and 30min). Then, images were captured with an Olympus FV1200 Confocal Microscope.

### 2.8 Phototoxicity of RGD-P-Ce6

A375 and NIH3T3 cells (4,000 cells per well in 96-well plates) were incubated with free Ce6, PEG-P-Ce6 and RGD-P-Ce6 (25, 50, 100, 200 and 400nM) at 37°C for 12hrs. Then cells were rinsed with fresh culture medium and photo-irradiated with 660nm laser (3.5mW/cm$^2$) for 30min. After 48hrs, cell viability was measured using Alamar blue Assay. Alamar blue was added into each well and incubated for 2 hrs, and then was detected using FLUOstar Omega (BMG Labtech, Germany). In addition, toxicity of free Ce6, PEG-P-Ce6 and RGD-P-Ce6 without light irradiation was also measured using Alamar Blue assay.

To investigate the effect of light dose on the photokilling of RGD-P-Ce6, A375 cells were incubated with 100nM of RGD-P-Ce6 in the dark for 12hrs and then rinsed twice with fresh culture media. After that, the cells were photo-irradiated with 660nm laser (3.5mW/cm$^2$) for 0, 5, 10, 20 and 30min (0, 1.05, 2.1, 4.2 and 6.3J/cm$^2$), respectively. After 48hrs, cell viability was measured using Alamar Blue Assay.

To investigate the effect of receptor inhibitor on the RGD-P-Ce6 mediated PDT, A375 cells were treated with RGD-P-Ce6 (50nM) in the absence and presence of the inhibitor cRGDfV (10μM) for 12hrs. Then cells were rinsed twice with fresh culture media and photo-irradiated with 660nm laser (3.5mW/cm$^2$) for 30min, respectively. After 48hrs, cell viability was measured using Alamar blue Assay.

### 2.9 Penetration and phototoxicity of RGD-P-Ce6 in tumor spheroids

For spheroids generation, A375 cells were seeded into ultra-low attachment 96-well round bottom plates (Thermo Scientific) at the density of 8,000 cells in 100μl media and cultured for 3 days. To detect the penetration of the nanoconjugates in spheroids, medium was replaced with fresh medium containing free Ce6 and RGD-P-Ce6 at the concentrations of 200, 400 and 800nM. After 24hrs, the spheroids were digested into single cells and the Ce6 fluorescence in A375 cells was detected by flow cytometry using BD LSR II. For confocal

imaging, the spheroids treated by free Ce6 and RGD-P-Ce6 were fixed in 4% paraformaldehyde and were then mounted on a slide with fluoromount G (Electron Microscopy Sciences, Hatfield, PA). The spheroids were imaged using Olympus FV1200 confocal microscope to collect Z stack images, preceding every 10μm until laser penetration faltered (~190μm in depth).

To examine the phototoxicity, A375 spheroids were treated with Ce6 and RGD-P-Ce6 (800nM) for 24hrs. Then the spheroids were rinsed with fresh culture medium and incubated for another 1hr before photo-irradiation (660nm laser, 3.5mW/cm$^2$ and 30min). Images of the spheroids were captured using microscope. Four days after photo-irradiation, cell viability of the spheroids was measured using Alamar Blue Assay.

### 2.10 Data analysis

Data are expressed as mean ± SD from three measurements unless otherwise noted. Statistical significance was evaluated using *t*-test for two-sample comparison or ANOVA followed by Dunnet's test for multiple comparisons. The data were analyzed with GraphPad Prism 5 (GraphPad Software, Inc., La Jolla, CA).

## 3. Results

### 3.1 Physicochemical characterization of RGD-P-Ce6

The zeta potential of PEG-P-Ce6 and RGD-P-Ce6 were +2.9mV and +0.8mV, respectively (Fig. 1b, Sfig. 2). The TEM image of RGD-P-Ce6 showed well dispersed spherical morphology (Fig. 1c). The average hydrodynamic diameter of PEG-P-Ce6 and RGD-P-Ce6 measured by DLS was 20nm and 28nm, respectively (Fig. 1a, Sfig. 3). The number of Ce6 linked to each dendrimer was estimated to be approximately 6.5 based on quantitation of Ce6 content in final product using UV spectrometry.

The UV/vis absorption of RGD-P-Ce6 showed two main peaks at 405 and 661nm (Sfig. 4), which was similar to free Ce6. The fluorescence of free Ce6 dissolved in methanol is significantly higher than that diluted by water, likely due to formation of aggregation in aqueous solution. The fluorescence of RGD-P-Ce6 in aqueous solution is higher than free Ce6 dissolved in water (Sfig. 5), which may indicate that conjugation to PAMAM dendrimer prevents intermolecular aggregation of Ce6 that dramatically decreases the Ce6 fluorescence.

To investigate the photo-activity of RGD-P-Ce6 in aqueous solution, the fluorescence of SOSG before and after photo-irradiation was measured. The singlet oxygen yield of RGD-P-Ce6 in aqueous media was approximately 2.5-fold higher than that of free Ce6 (Fig. 1d), indicating that conjugation of dendrimers prevented Ce6 aggregation and thus maintained its photo-activity. Photosensitizers are able to absorb light radiation and eventually transfer that energy to the substrate (type I) or molecular oxygen (type II) of photo oxygenation process. According to previous studies, free Ce6 or Ce6 conjugates/nanoparticles had a significant contribution from type II (singlet oxygen) mechanism for PDT effects.[23–25] The result of singlet oxygen production indicated that the photo-activity of RGD-P-Ce6 undergoes a type II mechanism.

### 3.2 Intracellular uptake of targeted nanoconjugates RGD-P-Ce6

Intracellular uptake of free Ce6, PEG-P-Ce6 and RGD-P-Ce6 was evaluated by incubating integrin αvβ3-expressing A375 cells with these molecules for 12hrs and then analysis using flow cytometry. The result in Fig. 2a showed that both RGD-P-Ce6 and PEG-P-Ce6 exhibited significant higher cellular uptake than free Ce6. There was 4.7-fold greater uptake of the targeted RGD-P-Ce6 as compared with the non-targeted PEG-P-Ce6 in A375 cells. A selective inhibitor of integrin αvβ3 (cRGDfV peptide, 10μM) effectively reduced the uptake of RGD-P-Ce6. In addition, uptake of free Ce6, PEG-P-Ce6 and RGD-P-Ce6 was also evaluated in integrin αvβ3-negative NIH3T3 cells. As seen in Fig. 2b, PEG-P-Ce6 and RGD-P-Ce6 showed similar cellular uptake and cRGD did not cause significant reduction of the RGD-P-Ce6 uptake. These observations support the concept that enhanced cellular uptake of RGD-P-Ce6 depends on integrin αvβ3 mediated endocytosis.

Endocytosis is the main pathway by which NPs enter cells. The result in Fig. 2c showed that cellular uptake of RGD-P-Ce6 by A375 cells was energy-dependent; as the uptake was reduced by 94.1% when it was performed at 4°C. Dynamin is a large guanosine triphosphatase which regulates both clathrin- and caveolae-mediated endocytosis, and small molecule dynasore can specifically inhibit dynamin.[26] In our experiment, dynasore reduced the cellular uptake of RGD-P-Ce6 by 98.3%, suggesting that endocytosis of RGD-P-Ce6 into A375 cells was dependent on clathrin and/or caveolae-mediated endocytosis. Chlorpromazine is a blocking agent of clathrin-coated pit formation. It decreased the RGD-P-Ce6 uptake by 74.3%, indicating the involvement of clathrin-mediated endocytosis in RGD-P-Ce6 uptake. Filipin and methyl-β-cyclodextrin are two special inhibitors of caveolae-mediated endocytosis. They had a moderate inhibition on the RGD-P-Ce6 uptake (10.3% and 19.1%), indicating that caveolae-associated endocytosis was also involved in RGD-P-Ce6 uptake but played a minor role. Amiloride and wortmannin, two specific inhibitors of macropinocytosis, did not have significant effects on RGD-P-Ce6 uptake, indicating that macropinocytosis may not be involved in cellular uptake of RGD-P-Ce6.

### 3.3 Intracellular localization of RGD-P-Ce6

Intracellular trafficking of RGD-P-Ce6 was studied using confocal microscopy. After 6-hr incubation, RGD-P-Ce6 was largely colocalized with the lysosomal marker Lysotracker green (Fig. 3), but not with the early endosome marker transferrin (Sfig. 6), indicating that RGD-P-Ce6 was transported to the late endosomes/lysosomes after cellular entry. RGD-P-Ce6 did not located in endoplasmic reticulum (ER) as there was little colocalization between RGD-P-Ce6 and ER Tracker Green (Sfig. 7).

### 3.4 Intracellular singlet oxygen detection during photo-irradiation

To detect the intracellular singlet oxygen generation, A375 cells were treated with CM-$H_2$DCFDA, a non-fluorescent molecule that can passively diffuse into cells. In the cells, its acetate groups are cleaved by intracellular esterase and subsequent oxidation yields a bright fluorescent probe that is trapped inside the cell. Fig. 4a showed that RGD-P-Ce6 induced production of ROS in A375 cells upon photo-irradiation, and the amount of ROS depended on the dose of photo-irradiation (Sfig. 8). In contrast to the increase in singlet oxygen generation, the intracellular RGD-P-Ce6 after photo-irradiation gradually decreased upon

photo-irradiation (Sfig. 9), indicating Ce6 were degraded by singlet oxygen that was produced by itself.

The similar results were obtained by using confocal microscopy. In the group treated by RGD-P-Ce6 and CM-$H_2$DCFDA but without photo-irradiation, most of the cells were dim. However, bright green fluorescence was observed in most cells after photo-irradiation (Fig. 4b).

### 3.5 Apoptosis mediated by RGD-P-Ce6

Cell apoptosis induced by RGD-P-Ce6 mediated PDT was detected using flow cytometry. Annexin V-FITC and PI were used as fluorescent probes to distinguish viable cells from apoptotic or dead cells. The results in Fig. 5 showed the different cells populations (viable (Annexin V-FITC$^-$/PI$^-$), early apoptotic (Annexin V-FITC$^+$/PI$^-$), and late-stage apoptotic or dead (Annexin V-FITC$^+$/PI$^+$) were induced by different treatments. After the cells were treated with either laser or RGD-P-Ce6 alone, over 97% of the cells were viable. Ten min after photo-irradiation, there were 4.4% early apoptotic cells and 1.8% dead cells, respectively. After 4 and 12 hrs post photo-irradiation, early apoptotic cells increased to 14.6% and 25.7%, respectively, and dead cells increased to 5.8% and 25.2%, respectively. As time going on, more apoptotic or dead cells appeared in the RGD-P-Ce6 group (Fig. 5 and Sfig. 10).

### 3.6 PDT mediated lysosomal leakage

To explore the mechanism of cell apoptosis, we examined the integrity of lysosomes in A375 cells after RGD-P-Ce6 treatment followed by photo-irradiation. The Alexa 488-dextran release-method was used to determine lysosomal leakage as dextran is trapped predominantly in the intact lysosomes.[27] As seen in Fig. 6, without photo-irradiation, dextran was confined to cytoplasmic vesicles as dots. However, obvious green fluorescence diffused into the whole cells when the cells were photo-irradiated with 660nm laser, indicating that the lysosomes were where oxidative stress was produced by PDT.

### 3.7 Cytotoxicity of RGD-P-Ce6 with or without photo-irradiation

To investigate the dark cytotoxicity, free Ce6, PEG-P-Ce6 and RGD-P-Ce6 were added into A375 cells at different concentrations (0.4, 0.8, 1.2, 1.6 and 2μM). The result showed that all of these three forms of Ce6 did not exhibit obvious cytotoxicity in dark (Sfig. 11).

In order to investigate the photo-cytotoxicity of free Ce6, PEG-P-Ce6 and RGD-P-Ce6, A375 and NIH3T3 cells were treated at different concentrations (25, 50, 100, 200, 400 and 800nM), and were then photo-irradiated with a 660nm laser (3.5mW/cm$^2$) for 30 min. The result in Fig. 7a indicated that there was almost no cell killing when A375 cells treated by free Ce6 with photo-irradiation, which may be due to the poor cellular uptake of free Ce6. However, when irradiated with 660nm laser, RGD-P-Ce6 showed significantly enhanced phototoxicity to A375 cells when compared to PEG-P-Ce6 and Ce6. In integrin αvβ3-negative NIH3T3 cells, PEG-P-Ce6 and RGD-P-Ce6 showed similar phototoxicity upon photo-irradiation (3.5mW/cm$^2$) (Fig. 7b).

To examine the effect of light dose on the phototoxicity of RGD-P-Ce6, A375 cells were illuminated with various light doses (0, 1.05, 2.1, 4.2 and 6.3J/cm$^2$) following 12-hr incubation with 100nM of RGD-P-Ce6. As shown in Sfig. 12, photokilling of A375 cells by RGD-P-Ce6 improved as light dose increased.

To examine the effect of integrin αvβ3 inhibitor on the RGD-P-Ce6 mediated PDT, A375 cells were treated with RGD-P-Ce6 in the absence and presence of cRGDfV (10μM). As shown in Sfig. 13, cRGDfV significantly reduced the phototoxicity of RGD-P-Ce6, indicating photokilling by RGD-P-Ce6 depends on integrin αvβ3-mediated cellular uptake.

### 3.8 Penetration of RGD-P-Ce6 in tumor spheroids

Penetration of Ce6 and RGD-P-Ce6 were examined in A375 tumor spheroids. The results in Fig. 8a and Sfig. 14 showed that RGD-P-Ce6 was found throughout the spheroids while the free Ce6 exhibited little fluorescence. In the group treated with free Ce6, the profile of the flow cytometry histogram shows that the distribution of the free Ce6 was homogeneous in spheroids but the level was quite low (Fig. 8b), indicating that free Ce6 could penetrate into the spheroids but the cellular uptake was poor. As shown in Fig. 8c, RGD-P-Ce6 (200nM) entered about 62.5% cells in spheroids. When the concentration increased to 400nM and 800nM, the percentage increased to 78% and 88.03%, respectively (Fig. 8d). With the same concentrations of 200, 400 and 800nM, RGD-P-Ce6 showed 40.8-, 58.7- and 79.3-folded higher cellular uptake than free Ce6, respectively. These results indicated that RGD-P-Ce6 can penetrate the spheroids deeply and then enter most of the cancer cells.

### 3.9 Phototoxicity of RGD-P-Ce6 in tumor spheroids

To evaluate PDT effects in tumor spheroids, A375 spheroids were treated with free Ce6 and RGD-P-Ce6 (800nM) for 24 hrs and were then irradiated with a 660nm laser. Before photo-irradiation, there was no obvious difference in control, free Ce6 and RGD-P-Ce6 groups (Fig. 9a). Images in RGD-P-Ce6 group showed that there was an obvious physical shrinking of the spheroids at Day 1 post photo-irradiation. The spheroids this group did not grow for 4 days after photo-irradiation (Fig. 9b). The Alamar blue cytotoxicity assay again showed significant cell death when compared with control and free Ce6 groups (Fig. 9c). No significant difference between untreated and free Ce6 groups was detected in serial microscopic observations and the Alamar blue assay.

## 4. Discussion

To overcome the problems of self-aggregation in aqueous solution and poor tumor delivery of hydrophobic photosensitizers, we aimed to construct targeted nanoconjugates that are small and non-cytotoxic in dark. Thus, PAMAM dendrimer, Ce6, and cRGD peptides were selected as the carrier, therapeutic agent, and targeting ligand, respectively. The RGD-P-Ce6 nanoconjugates exhibited monodispersed size distribution at 28nm and nearly neutral surface charge (+0.8mV). The size of the nanoconjugates is large enough to avoid quick renal filtration and is also smaller than conventional NPs so that they may penetrate deeply into tumor tissues. In addition, the neutral charge of RGD-P-Ce6 can avoid nonspecific

adsorption of proteins on the nanoconjugates surface, which may lead to formation of aggregates and thereafter quick clearance from the reticular-endothelial system.

The poor internalization of free Ce6 in serum-containing medium may be due to strong binding of Ce6 to serum proteins. In serum-free Opti-MEM media, cellular uptake of free Ce6 was dramatically higher than that in serum-containing medium (Sfig. 15). Uptake of RGD-P-Ce6 was not affected in the presence of serum (Sfig. 16), indicating that it can avoid nonspecific protein binding and thus exhibit superior cancer cell uptake via endocytosis.

Ideally, photosensitizers should be nontoxic in dark to avoid side effects. On the other hand, high phototherapeutic efficacy is desirable to completely damage the target cells in disease tissues. RGD-P-Ce6 exhibited no toxicity in dark even at the concentration of 2μM, while upon photo-irradiation, the $IC_{50}$ of RGD-P-Ce6 was as low as 25nM (Fig. 7a). When the cancer cells were incubated with 400nM RGD-P-Ce6 and photo-irradiated for 30min, the viability dramatically decreased to less than 5%. However, at the same concentration of free Ce6 (400nM), there was no photo-therapeutic effect. The results indicated that RGD-P-Ce6 is an effective system to deliver Ce6 to cancer cells to perform PDT.

Previous studies showed that free Ce6 accumulates in several subcellular sites including plasma membrane, ER, and lysosome.[28] When Ce6 is conjugated to RGD functionalized PAMAM dendrimer, the subcellular localization is limited. RGD-P-Ce6 is internalized by cancer cells mainly via the clathrin mediated endocytosis pathway. Upon cellular entry, RGD-P-Ce6 entered the late endosomes and lysosomes (Fig. 3). In the lysosomes, singlet oxygen generation upon photo-irradiation could be detected in a dose dependent manner of photo-irradiation. Singlet oxygen generated in lysosomes causes the destruction of the lysosome, leakage of lysosomal contents and finally induction of apoptosis.[29, 30] Apoptotic cells can be removed by innate immune system and macrophages and thus tissue damage is therefore limited to the photo-irradiated area.[31]

The problem of limited penetration of NPs in tumors has recently received growing attention. Some studies have pointed to a minimal particle size of less than 50 nm as a requirement for NP penetration.[13, 18] Particle size has a substantial impact on pharmacokinetics and biodistribution of NPs, especially on their distribution to tumor sites. NPs with the size between 7 to 300nm may have long circulation time in blood because of reduced clearance through renal filtration and by the reticuloendothelial system.[32] These NPs may have better distribution in leaky sites of tumors due to the EPR effect.[33] However, larger particles may have poor delivery to less leaky sites in highly heterogeneous tumor tissues.[34] In addition, tumor penetration of larger NPs is largely constrained by narrow spacing between tumor cells [35, 36], presence of extracellular matrix, and high interstitial fluid pressure.[34, 37] Taken together, smaller NPs (10–50nm) may provide a superior delivery system for tumor targeting. In addition, some studies indicated that surface charge of NPs also played an important role in spheroids penetration.[38, 39] It showed that negative and neutral NPs exhibit greater penetration compared with cationic NPs owing to the lack of electrostatic binding to ECM or cells.[40] Moreover, inclusion of peptide RGD was also reported to act as a tumor targeting moiety while concurrently enhancing tumor tissue penetration.[39, 41] The RGD-P-Ce6 nanoconjugates are targeted neutral NPs with an

average size smaller than 50 nm, and thus appear to possess most of the commonly characteristics that are necessary for deep tumor penetration. Our initial study using tumor spheroids has confirmed excellent tumor penetration of the targeted dendritic nanoconjugates.

## 5. Conclusion

In this study, we successfully prepared targeted nanoconjugates that have shown superior PDT effects in cellular tumor models. The nanoconjugates are small in size, neutral and non-toxic in dark. The RGD functionalized nanoconjugates demonstrated enhanced cellular internalization via receptor-mediated endocytosis. In addition, the targeted nanoconjugates also exhibited efficient penetration into tumor spheroids. Upon photo-irradiation, the nanoconjugates produced sufficient singlet oxygen to induce cell apoptosis in both cancer cells monolayer and 3-D spheroids. As a result of their great cellular delivery, small size, and lack of dark cytotoxicity, the nanoconjugates may provide an effective tool for targeted PDT of solid tumors.

## Supplementary Material

Refer to Web version on PubMed Central for supplementary material.

## Acknowledgments

This work was supported by NIH grants 5U54CA151652 and 5R01CA151964 and an Innovation Award from the University Cancer Research Fund (UNC Lineberger Comprehensive Cancer Center). Ahu Yuan was sponsored by the China Scholarship Council.

## References

1. Ge JC, Lan MH, Zhou BJ, Liu WM, Guo L, Wang H, et al. A graphene quantum dot photodynamic therapy agent with high singlet oxygen generation. Nat Commun. 2014; 5
2. Mitsunaga M, Ogawa M, Kosaka N, Rosenblum LT, Choyke PL, Kobayashi H. Cancer cell-selective in vivo near infrared photoimmunotherapy targeting specific membrane molecules. Nature medicine. 2011; 17:1685–91.
3. Chu M, Li H, Wu Q, Wo F, Shi D. Pluronic-encapsulated natural chlorophyll nanocomposites for in vivo cancer imaging and photothermal/photodynamic therapies. Biomaterials. 2014; 35:8357–73. [PubMed: 25002262]
4. Gibot L, Lemelle A, Till U, Moukarzel B, Mingotaud AF, Pimienta V, et al. Polymeric micelles encapsulating photosensitizer: structure/photodynamic therapy efficiency relation. Biomacromolecules. 2014; 15:1443–55. [PubMed: 24552313]
5. Chen Z, Xu P, Chen J, Chen H, Hu P, Chen X, et al. Zinc phthalocyanine conjugated with the amino-terminal fragment of urokinase for tumor-targeting photodynamic therapy. Acta biomaterialia. 2014
6. Shi J, Liu Y, Wang L, Gao J, Zhang J, Yu X, et al. A tumoral acidic pH-responsive drug delivery system based on a novel photosensitizer (fullerene) for in vitro and in vivo chemo-photodynamic therapy. Acta biomaterialia. 2014; 10:1280–91. [PubMed: 24211343]
7. Jeong H, Huh M, Lee SJ, Koo H, Kwon IC, Jeong SY, et al. Photosensitizer-conjugated human serum albumin nanoparticles for effective photodynamic therapy. Theranostics. 2011; 1:230–9. [PubMed: 21562630]
8. Jiang C, Cheng H, Yuan A, Tang X, Wu J, Hu Y. Hydrophobic IR780 encapsulated in biodegradable human serum albumin nanoparticles for photothermal and photodynamic therapy. Acta biomaterialia. 2015; 14:61–9. [PubMed: 25463484]

9. Park H, Na K. Conjugation of the photosensitizer Chlorin e6 to pluronic F127 for enhanced cellular internalization for photodynamic therapy. Biomaterials. 2013; 34:6992–7000. [PubMed: 23777915]
10. Oh IH, Min HS, Li L, Tran TH, Lee YK, Kwon IC, et al. Cancer cell-specific photoactivity of pheophorbide a-glycol chitosan nanoparticles for photodynamic therapy in tumor-bearing mice. Biomaterials. 2013; 34:6454–63. [PubMed: 23755832]
11. Mallikaratchy P, Tang Z, Tan W. Cell specific aptamer-photosensitizer conjugates as a molecular tool in photodynamic therapy. Chem Med Chem. 2008; 3:425–8. [PubMed: 18058891]
12. Lee SJ, Koo H, Jeong H, Huh MS, Choi Y, Jeong SY, et al. Comparative study of photosensitizer loaded and conjugated glycol chitosan nanoparticles for cancer therapy. Journal of controlled release: official journal of the Controlled Release Society. 2011; 152:21–9. [PubMed: 21457740]
13. Wong C, Stylianopoulos T, Cui J, Martin J, Chauhan VP, Jiang W, et al. Multistage nanoparticle delivery system for deep penetration into tumor tissue. Proc Natl Acad Sci U S A. 2011; 108:2426–31. [PubMed: 21245339]
14. Miele E, Spinelli GP, Miele E, Tomao F, Tomao S. Albumin-bound formulation of paclitaxel (Abraxane ABI-007) in the treatment of breast cancer. Int J Nanomedicine. 2009; 4:99–105. [PubMed: 19516888]
15. Petros RA, DeSimone JM. Strategies in the design of nanoparticles for therapeutic applications. Nature reviews Drug discovery. 2010; 9:615–27.
16. Sugahara KN, Teesalu T, Karmali PP, Kotamraju VR, Agemy L, Girard OM, et al. Tissue-penetrating delivery of compounds and nanoparticles into tumors. Cancer cell. 2009; 16:510–20. [PubMed: 19962669]
17. Carver K, Ming X, Juliano RL. Multicellular Tumor Spheroids as a Model for Assessing Delivery of Oligonucleotides in Three Dimensions. Mol Ther-Nucl Acids. 2014; 3
18. Kim HJ, Takemoto H, Yi Y, Zheng M, Maeda Y, Chaya H, et al. Precise engineering of siRNA delivery vehicles to tumors using polyion complexes and gold nanoparticles. Acs Nano. 2014; 8:8979–91. [PubMed: 25133608]
19. Skupin-Mrugalska P, Piskorz J, Goslinski T, Mielcarek J, Konopka K, Duzgunes N. Current status of liposomal porphyrinoid photosensitizers. Drug discovery today. 2013; 18:776–84. [PubMed: 23591149]
20. Niu G, Chen X. Why integrin as a primary target for imaging and therapy. Theranostics. 2011; 1:30–47. [PubMed: 21544229]
21. Gao H, Yang Z, Zhang S, Cao S, Shen S, Pang Z, et al. Ligand modified nanoparticles increases cell uptake, alters endocytosis and elevates glioma distribution and internalization. Scientific reports. 2013; 3:2534. [PubMed: 23982586]
22. Tian J, Ding L, Xu HJ, Shen Z, Ju H, Jia L, et al. Cell-specific and pH-activatable rubyrin-loaded nanoparticles for highly selective near-infrared photodynamic therapy against cancer. Journal of the American Chemical Society. 2013; 135:18850–8. [PubMed: 24294991]
23. Wang J, Zhu G, You M, Song E, Shukoor MI, Zhang K, et al. Assembly of aptamer switch probes and photosensitizer on gold nanorods for targeted photothermal and photodynamic cancer therapy. ACS nano. 2012; 6:5070–7. [PubMed: 22631052]
24. Kim H, Kim Y, Kim IH, Kim K, Choi Y. ROS-Responsive Activatable Photosensitizing Agent for Imaging and Photodynamic Therapy of Activated Macrophages. Theranostics. 2013; 4:1–11. [PubMed: 24396511]
25. Huang L, Xuan Y, Koide Y, Zhiyentayev T, Tanaka M, Hamblin MR. Type I and Type II mechanisms of antimicrobial photodynamic therapy: an in vitro study on gram-negative and gram-positive bacteria. Lasers in surgery and medicine. 2012; 44:490–9. [PubMed: 22760848]
26. Macia E, Ehrlich M, Massol R, Boucrot E, Brunner C, Kirchhausen T. Dynasore, a cell-permeable inhibitor of dynamin. Dev Cell. 2006; 10:839–50. [PubMed: 16740485]
27. Petersen NH, Olsen OD, Groth-Pedersen L, Ellegaard AM, Bilgin M, Redmer S, et al. Transformation-associated changes in sphingolipid metabolism sensitize cells to lysosomal cell death induced by inhibitors of acid sphingomyelinase. Cancer cell. 2013; 24:379–93. [PubMed: 24029234]

28. Mojzisova H, Bonneau S, Vever-Bizet C, Brault D. Cellular uptake and subcellular distribution of chlorin e6 as functions of pH and interactions with membranes and lipoproteins. Biochimica et biophysica acta. 2007; 1768:2748–56. [PubMed: 17692283]
29. Guicciardi ME, Leist M, Gores GJ. Lysosomes in cell death. Oncogene. 2004; 23:2881–90. [PubMed: 15077151]
30. Boya P, Kroemer G. Lysosomal membrane permeabilization in cell death. Oncogene. 2008; 27:6434–51. [PubMed: 18955971]
31. Agostinis P, Berg K, Cengel KA, Foster TH, Girotti AW, Gollnick SO, et al. Photodynamic therapy of cancer: an update. CA: a cancer journal for clinicians. 2011; 61:250–81. [PubMed: 21617154]
32. Juliano R, Bauman J, Kang H, Ming X. Biological barriers to therapy with antisense and siRNA oligonucleotides. Mol Pharm. 2009; 6:686–95. [PubMed: 19397332]
33. Matsumura Y, Maeda H. A new concept for macromolecular therapeutics in cancer chemotherapy: mechanism of tumoritropic accumulation of proteins and the antitumor agent smancs. Cancer research. 1986; 46:6387–92. [PubMed: 2946403]
34. Ruenraroengsak P, Cook JM, Florence AT. Nanosystem drug targeting: Facing up to complex realities. Journal of controlled release: official journal of the Controlled Release Society. 2010; 141:265–76. [PubMed: 19895862]
35. Ishida T, Kiwada H. Alteration of tumor microenvironment for improved delivery and intratumor distribution of nanocarriers. Biological & pharmaceutical bulletin. 2013; 36:692–7. [PubMed: 23649327]
36. Nagano S, Perentes JY, Jain RK, Boucher Y. Cancer cell death enhances the penetration and efficacy of oncolytic herpes simplex virus in tumors. Cancer research. 2008; 68:3795–802. [PubMed: 18483263]
37. Florence AT. “Targeting” nanoparticles: the constraints of physical laws and physical barriers. Journal of controlled release: official journal of the Controlled Release Society. 2012; 164:115–24. [PubMed: 22484196]
38. Grainger SJ, Serna JV, Sunny S, Zhou Y, Deng CX, El-Sayed ME. Pulsed ultrasound enhances nanoparticle penetration into breast cancer spheroids. Molecular pharmaceutics. 2010; 7:2006–19. [PubMed: 20957996]
39. Ming X, Carver K, Wu L. Albumin-based nanoconjugates for targeted delivery of therapeutic oligonucleotides. Biomaterials. 2013; 34:7939–49. [PubMed: 23876758]
40. Sofou S. Surface-active liposomes for targeted cancer therapy. Nanomedicine. 2007; 2:711–24. [PubMed: 17976032]
41. Carver K, Ming X, Juliano RL. Multicellular tumor spheroids as a model for assessing delivery of oligonucleotides in three dimensions. Molecular therapy Nucleic acids. 2014; 3:e153. [PubMed: 24618852]

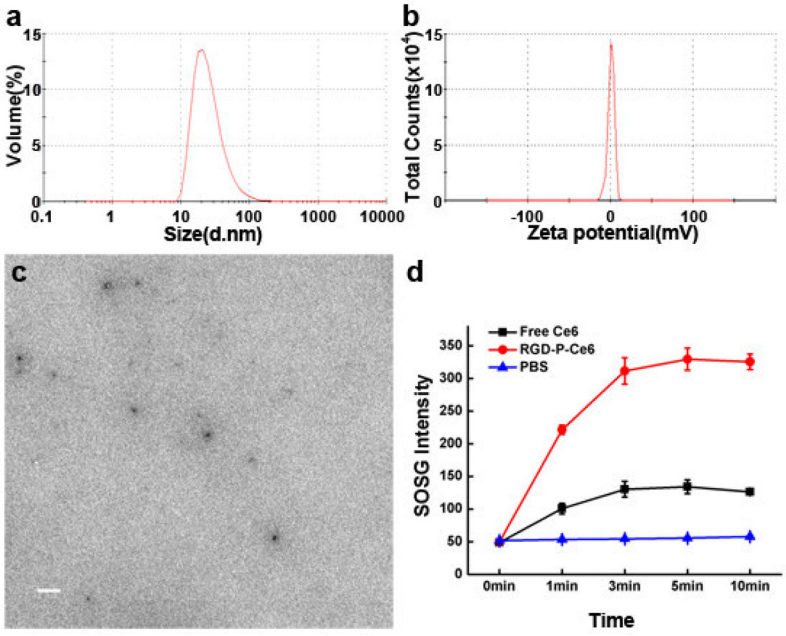


**Figure 1.**

Characterization of the targeted nanoconjugates RGD-P-Ce6. (a) Particle size distribution and (b) Zeta potential. (c) TEM image of RGD-P-Ce6. Scale bar, 100nm. (d) Change in SOSG fluorescence due to the generation of singlet oxygen by free Ce6 and RGD-P-Ce6 in PBS. PBS with SOSG was photo irradiated for 0, 1, 3, 5 and 10min and set as a negative control (n=3).

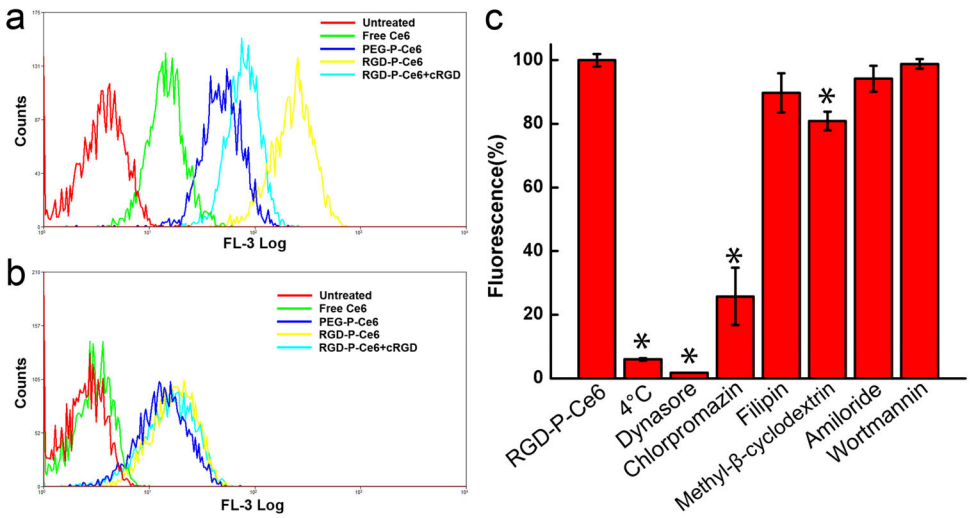


**Figure 2.**

Cellular uptake of free Ce6, PEG-P-Ce6 and RGD-P-Ce6 in A375 cells (a) and NIT3T3 cells (b). (c) Cellular uptake of RGD-P-Ce6 in the presence of various endocytic pathway inhibitors. A375 cells were pretreated with the inhibitors 0.5h prior to the incubation of RGD-P-Ce6 (n=3), * $p<0.05$.

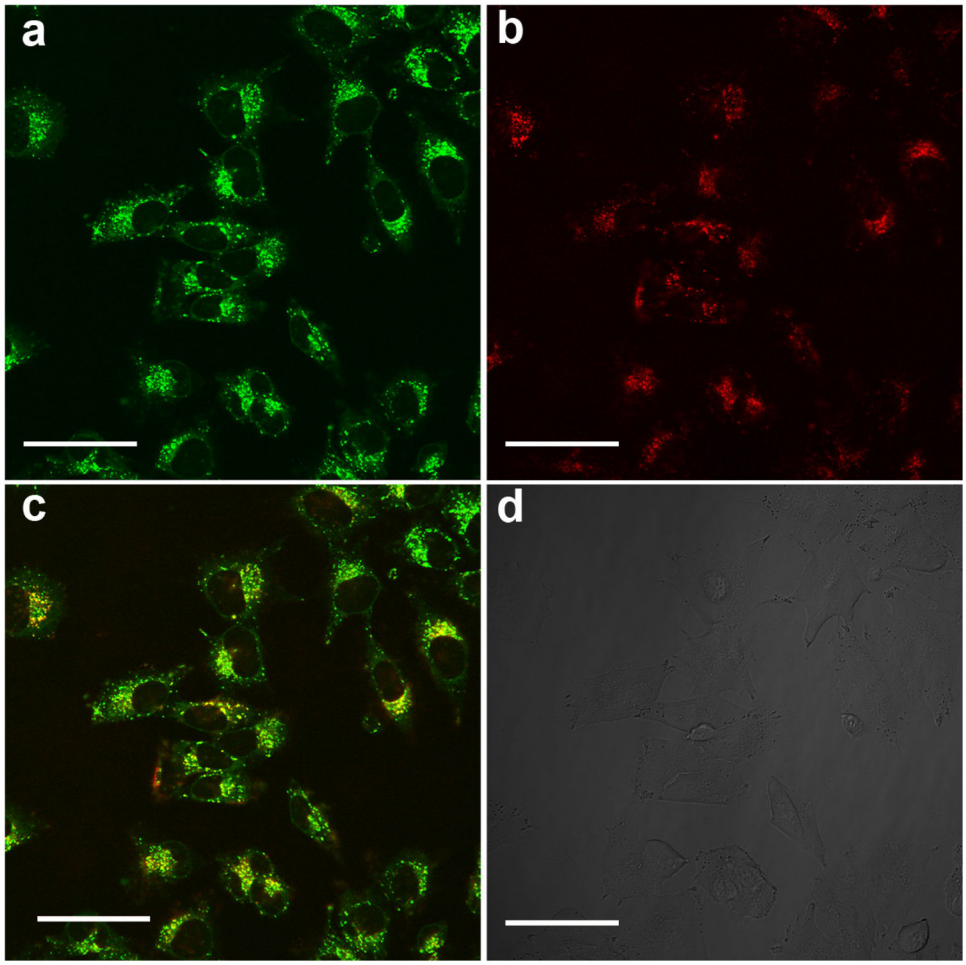


**Figure 3.**

Confocal fluorescence microscopy of A375 cells after treatment with RGD-P-Ce6 and Lysotracker Green. (a) Lysosomes labelled by Lysotracker green, (b) RGD-P-Ce6, (c) yellow regions indicate localization of RGD-P-Ce6 in the lysosomes and (d) DIC. Scale bar, 50μm.

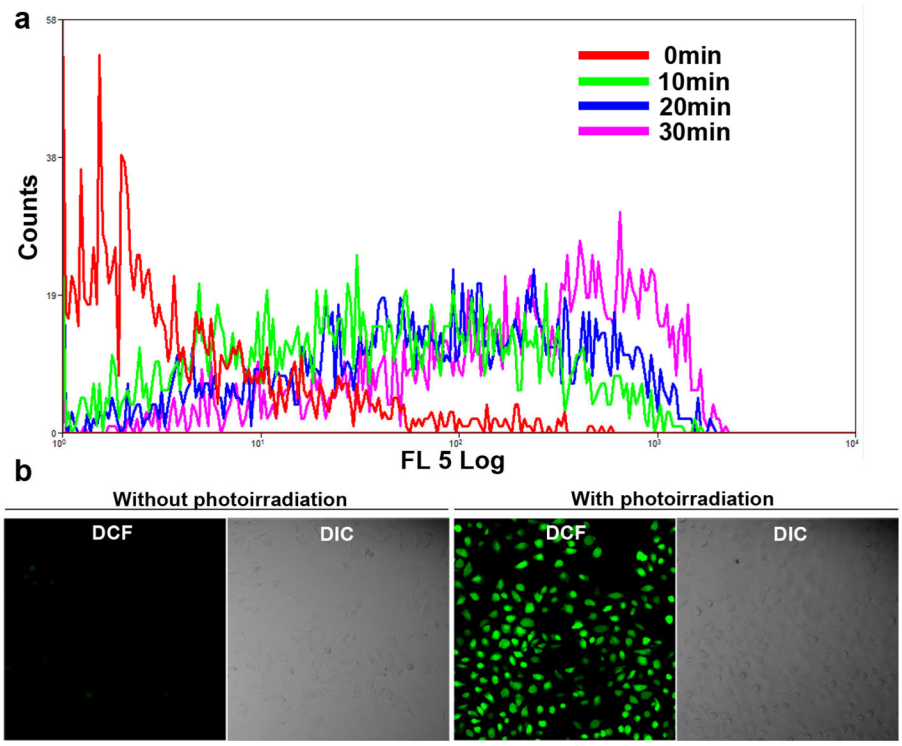


**Figure 4.**

Intracellular singlet oxygen. (a) Flow cytometry detection and (b) Confocal images of ROS generation during RGD-P-Ce6 mediated PDT with a cellular ROS probe, CM-$H_2$DCFDA.

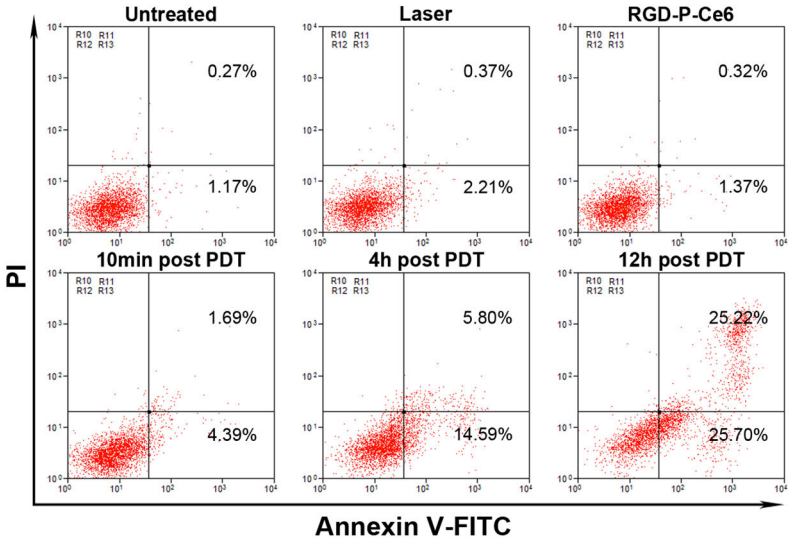


**Figure 5.**
Flow cytometry analysis of A375 cells apoptosis induced by RGD-P-Ce6 mediated PDT.

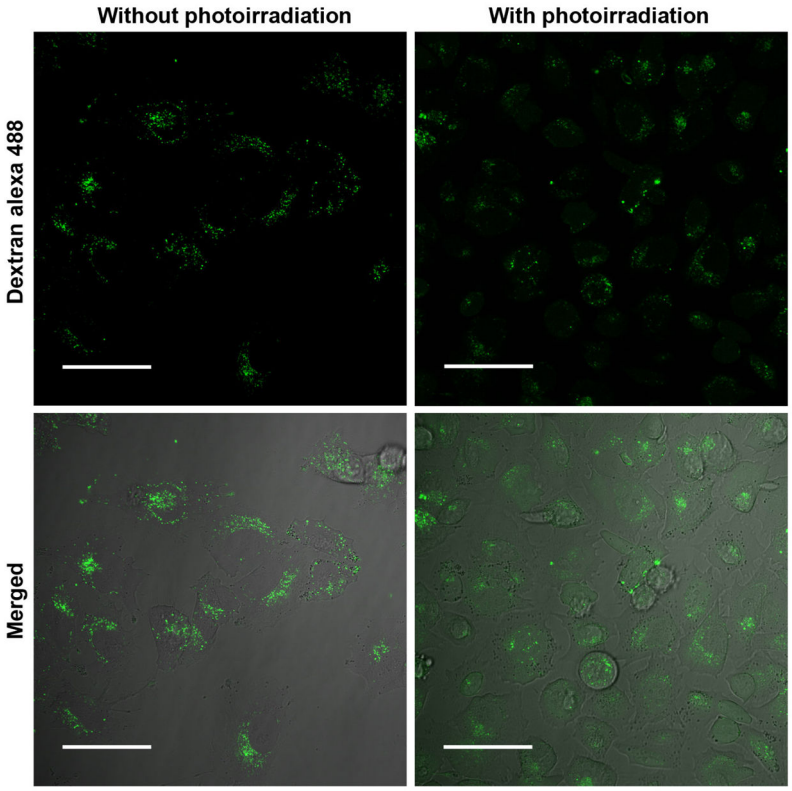


**Figure 6.**
Re-distribution of dextran-Alexa 488 induced by RGD-P-Ce6 mediated PDT. Scale bar, 50μm.

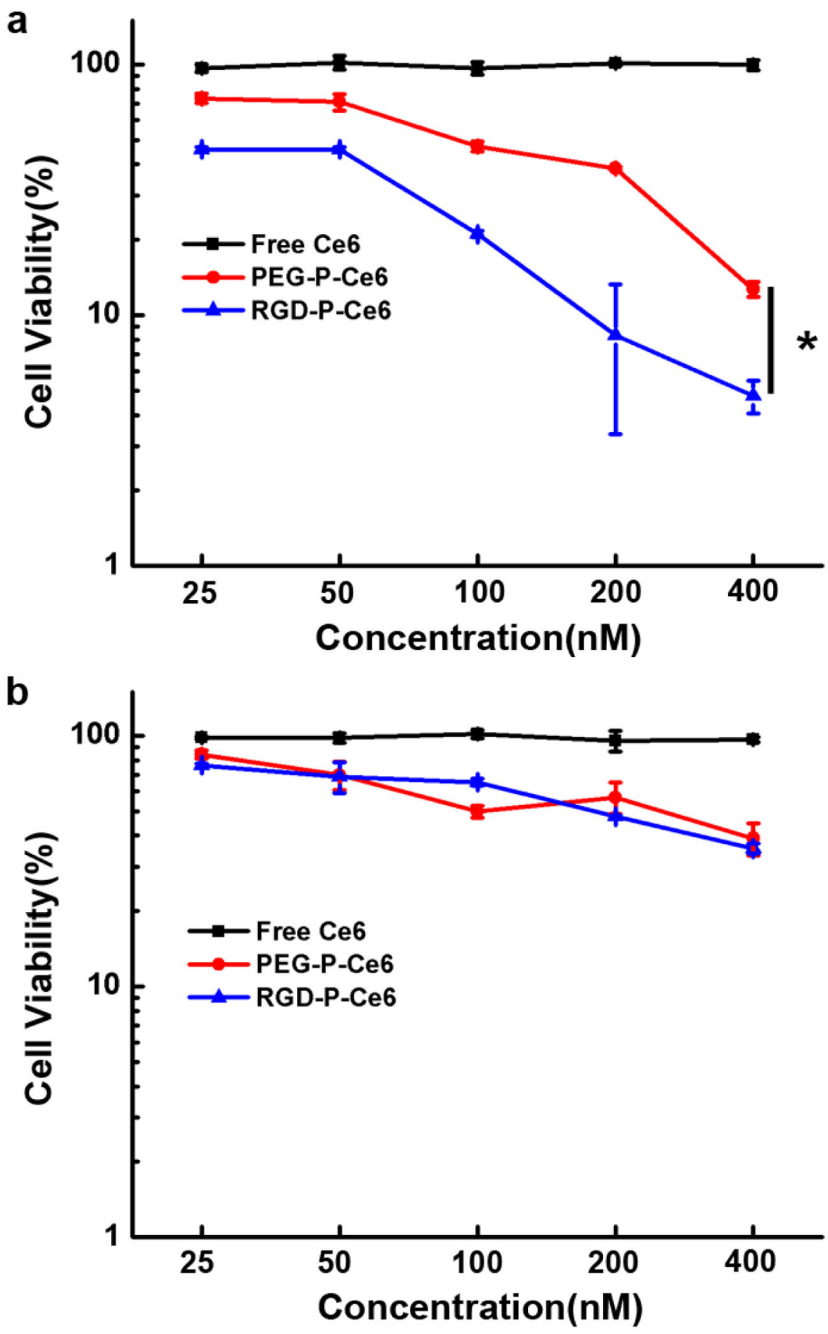


**Figure 7.**

In vitro phototoxicity of free Ce6, PEG-P-Ce6 and RGD-P-Ce6 in A375 cells (a) and NIH3T3 cells (b), n=4, * $p<0.05$.

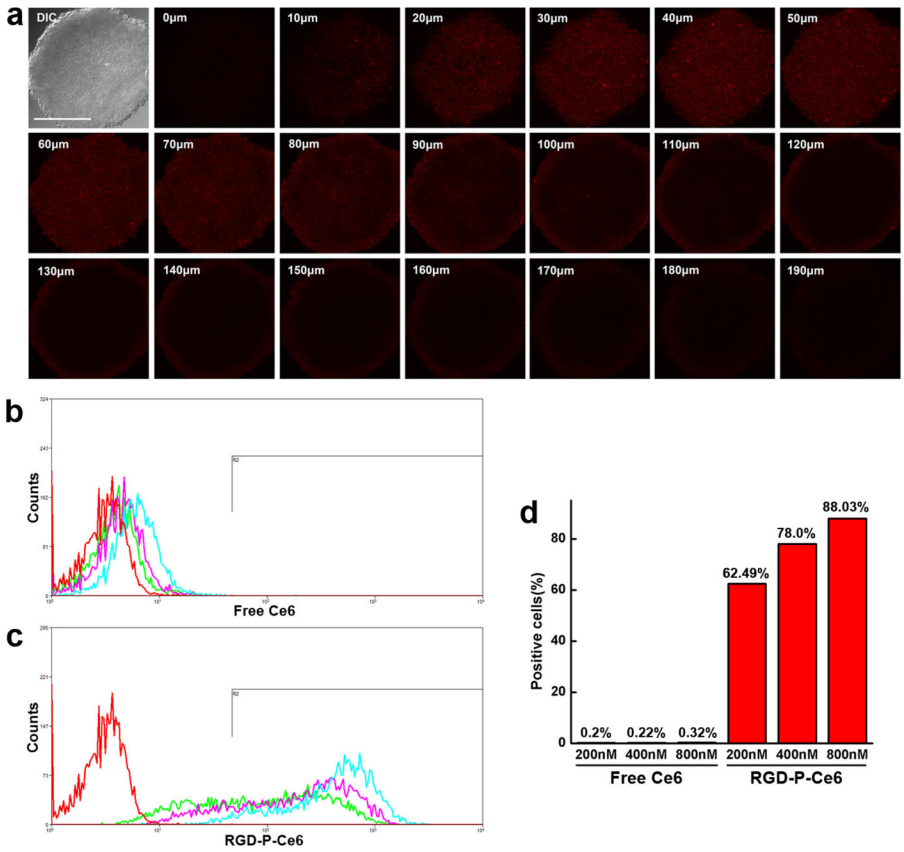


**Figure 8.**

(a) Z-Stack confocal microscopy images of A375 tumor spheroids treated by RGD-P-Ce6 (800nM) for 24 hrs. Scale bar, 300μm. (b) Flow cytometry of the digested cells of tumor spheroids treated by free Ce6 (200,400 and 800nM) for 24 hrs. (c) Flow cytometry of the digested cells of tumor spheroids treated by RGD-P-Ce6 (200,400 and 800nM) for 24 hrs. (d) Percentage of A375 cells in spheroids labelled by free Ce6 and RGD-P-Ce6.

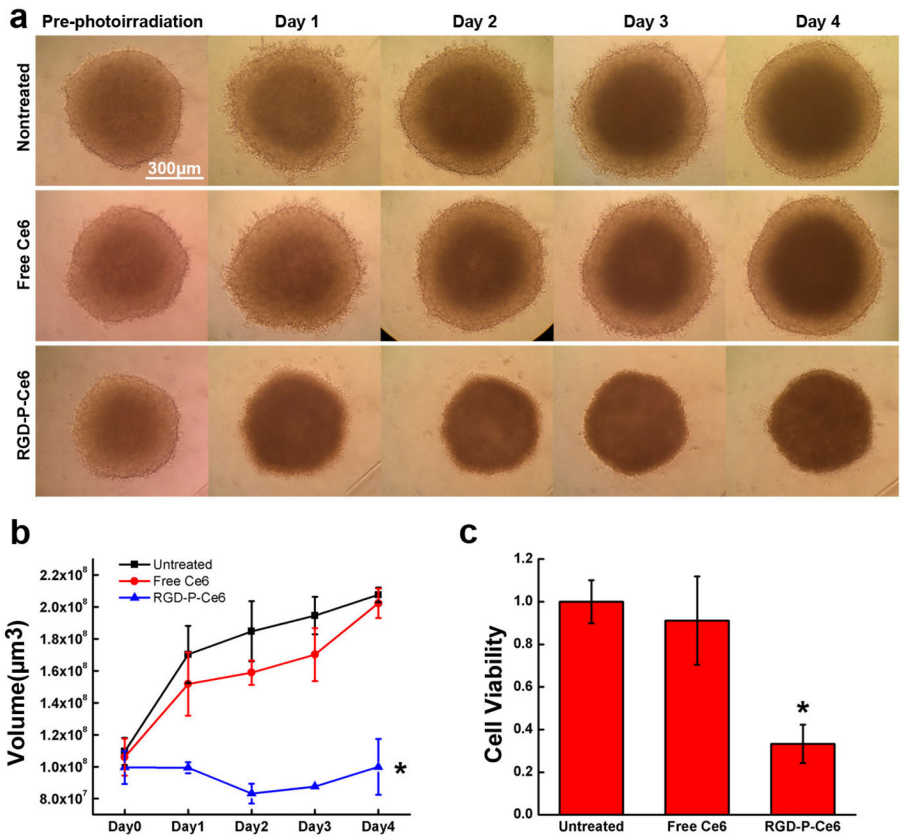


**Figure 9.**

Tumor spheroids. Images (a), volume (b) and cell viability (c) of tumor spheroids treated by free Ce6 and RGD-P-Ce6 mediated PDT. Untreated spheroids photo-irradiated by laser were set as control (n=3), Scale bar, 300μm, * $p<0.05$.